Proton and deuteron rapidity distributions and nuclear stopping in ^{96}Ru(^{96}Zr)+^{96}Ru(^{96}Zr) collisions at 400*A* MeV

B. Hong,[9,*] Y. J. Kim,[9] D. H. Kang,[9] Y. Leifels,[6] F. Rami,[10] B. de Schauenburg,[10] K. S. Sim,[9] J. P. Alard,[3] A. Andronic,[4,1] V. Barret,[3] Z. Basrak,[12] N. Bastid,[3] G. Berek,[2] R. Čaplar,[12] P. Crochet,[3] A. Devismes,[4] P. Dupieux,[3] M. Dželalija,[12] C. Finck,[4] Z. Fodor,[2] A. Gobbi,[4] Yu. Grishkin,[7] O. N. Hartmann,[4] N. Herrmann,[6] K. D. Hildenbrand,[4] J. Kecskemeti,[2] M. Kirejczyk,[11] P. Koczon,[4] M. Korolija,[12] R. Kotte,[5] T. Kress,[4] R. Kutsche,[4] A. Lebedev,[7] X. Lopez,[3] W. Neubert,[5] D. Pelte,[6] M. Petrovici,[1] W. Reisdorf,[4] D. Schűll,[4] Z. Seres,[2] B. Sikora,[11] V. Simion,[1] K. Siwek-Wilczyńska,[11] V. Smolyankin,[7] M. R. Stockmeier,[6] G. Stoicea,[1] P. Wagner,[10] K. Wiśniewski,[4] D. Wohlfarth,[5] I. Yushmanov,[8] and A. Zhilin[7]

(FOPI Collaboration)

[1]*Institute for Nuclear Physics and Engineering, Bucharest, Romania*
[2]*KFKI Research Institute for Particle and Nuclear Physics, Budapest, Hungary*
[3]*Laboratoire de Physique Corpusculaire, IN2P3/CNRS, and Université Blaise Pascal, Clermont-Ferrand, France*
[4]*Gesellschaft für Schwerionenforschung, Darmstadt, Germany*
[5]*Forschungszentrum Rossendorf, Dresden, Germany*
[6]*Physikalisches Institut der Universität Heidelberg, Heidelberg, Germany*
[7]*Institute for Theoretical and Experimental Physics, Moscow, Russia*
[8]*Kurchatov Institute, Moscow, Russia*
[9]*Korea University, Seoul, Korea*
[10]*Institut de Recherches Subatomiques and Université Louis Pasteur, Strasbourg, France*
[11]*Institute of Experimental Physics, Warsaw University, Poland*
[12]*Ruder Bošković Institute, Zagreb, Croatia*

(Received 2 May 2002; published 3 September 2002)

We present the centrality dependence of proton and deuteron rapidity distributions in Ru+Ru collisions at 400*A* MeV. Data are compared with isospin quantum molecular dynamics (IQMD) calculations under various assumptions on the nucleon-nucleon cross section in the medium. The rapidity spectra of both particles can be reproduced by IQMD with a free nucleon-nucleon cross section for the most central collisions. The ratio of baryon rapidity distributions in isospin asymmetric collision systems shows incomplete mixing and partial transparency of the projectile and target nuclei at this beam energy.

DOI: 10.1103/PhysRevC.66.034901 PACS number(s): 25.75.Dw, 25.75.Ld

I. INTRODUCTION

Heavy-ion collisions are the only method, which is presently available in the laboratory, to produce a large volume of the excited nuclear matter state [1–3]. Production of such an abnormal state is essential to investigate not only the gross characteristics of nuclear matter, but also the basic properties of quantum chromodynamics (QCD), the theory of strong interaction. The interests of the field include the hydrodynamic behavior of bulk nuclear matter [4,5] as well as the in-medium properties of hadrons in a dense and hot environment [6,7]. Several experimental observables have been proposed as sensitive probes of various aspects of dense and hot nuclear matter, i.e., the nuclear equation of state (EoS), in-medium nucleon-nucleon cross section (σ_{NN}), and the restoration of spontaneously broken chiral symmetry.

The degree of nuclear stopping in heavy-ion collisions is one of the essential observables which are necessary to understand the basic reaction dynamics; it is crucial information for estimating the energy and particle densities of the compressed nuclear matter at an early stage of the participant fireball. It is also closely related to the question of whether the (at least) local equilibrium model [8,9] is valid or a more elaborate nonequilibrium transport approach [10,11] is required for a description of the fireball. In many cases, nuclear stopping has been studied by baryon rapidity distributions at various beam energy ranges [12–16]. At energies larger than 1*A* GeV the experimental data show that these distributions are not compatible with the assumption of an isotropically expanding source [12–16]. The origin of this observation has become one of the most discussed subjects, since very similar rapidity distributions can be produced by transparency or the longitudinal expansion after thermal equilibrium of projectile and target nucleons. The resolution of this ambiguity in a model-independent way is rather difficult.

One idea to resolve it is utilizing nuclei of the same mass but a different neutron-to-proton ratio N/Z (''isospin mixing'') to distinguish several possibilities for nuclear stopping [17,18]. The advantage is that one can extract information on nuclear stopping directly from experimental data independent of a comparison with models. However, theoretical models using isospin mixing predict contradictory nuclear stopping phenomena. For example, the isospin quantum molecular dynamics (IQMD) model which considers isospin degrees of freedom into σ_{NN} as well as Coulomb interactions predicts transparency in ^{50}Cr+^{48}Ca collisions from 150*A* MeV to 1.5*A* GeV. This model also predicts that the

*Email address: bhong@korea.ac.kr

transparency becomes more pronounced at higher beam energies, and that the degree of nuclear stopping (or isospin equilibrium) depends on σ_{NN} to a large extent. The sensitivity of the isospin asymmetry on σ_{NN} has been demonstrated by showing a transition from transparency to rebound as σ_{NN} increases by a factor of 5 in IQMD [17]. On the other hand, Hombach *et al.* claimed that there is more stopping at higher beam energies up to 2*A* GeV within the framework of the coupled-channel Boltzmann-Uehling-Uhlenbeck (CBUU) model [19].

Experimentally, the isospin-mixing method has been applied to central nucleus-nucleus collisions at low beam energies only (up to 53*A* MeV) [20,21]. Below 40*A* MeV the isotope ratios of light fragments increase with the combined N/Z ratio of target and projectile, supporting the assumption of the isospin being equilibrated prior to the emission of fragments. Above 40*A* MeV, however, the isotope ratios depend on the respective N/Z ratio of target and projectile, especially near the target and projectile rapidities, thus remembering the entrance channel. In the present experiment our collaboration has extended the idea of isospin mixing to the higher energies of 400*A* MeV and 1.5*A* GeV. The first results at 400*A* MeV with two isospin tracer observables, namely, the ^{3}H/^{3}He ratio in the forward hemisphere and the protonlike (proton and deuteron) particle ratio in the backward hemisphere in the center-of-mass (c.m.) frame, were published recently [22].

In this paper, we will use both the centrality dependence of the baryon rapidity distributions and the comparison of those in isospin asymmetric systems in order to examine the nuclear stopping phenomenon in heavy-ion collisions at 400*A* MeV. Furthermore, we will compare experimental data with IQMD calculations and study whether the model can properly reproduce the degree of nuclear stopping.

II. EXPERIMENT

The experiment was performed at the heavy-ion synchrotron SIS of GSI in Darmstadt, Germany, using the FOPI detector, which is described in detail elsewhere [23–25]. We used two stable isobaric nuclei with the largest possible N/Z difference in the Periodic Table for relatively large masses ($^{96}_{44}$Ru and $^{96}_{40}$Zr). Data for four projectile-target combinations were taken in order to examine the isospin dependence of various physical observables: Ru (beam)+Zr (target), Zr (beam)+Ru (target) as well as Ru+Ru and Zr+Zr collisions. Measuring four reactions under the same experimental conditions has the advantage of eliminating the systematic errors in the ratio of the rapidity spectra. The targets were 431 mg/cm^2 and 380 mg/cm^2 thick in the case of Zr and Ru, respectively. All reactions were studied at 400*A* MeV and 1.5*A* GeV. In this paper only the results at 400*A* MeV will be discussed. Note that the nucleon-nucleon reaction cross section at and below 400*A* MeV is dominated by elastic scattering.

For the tracking of charged particles we use two drift chambers, CDC and HELITRON. Both chambers are placed inside a uniform solenoidal magnetic field of 0.6 T. The CDC covers the laboratory polar angles $\theta_L = 32° - 140°$, while the

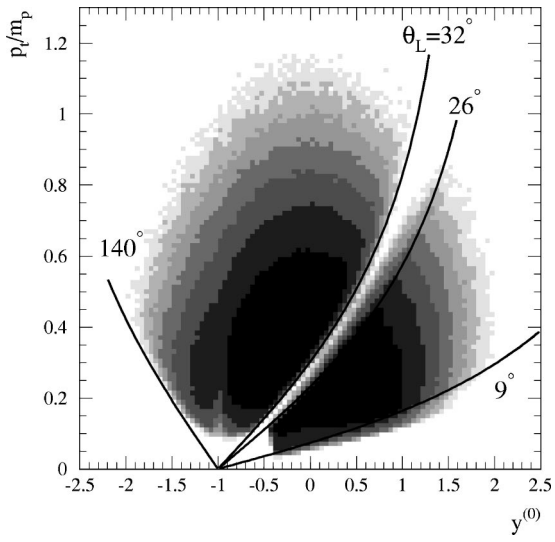

FIG. 1. Acceptance plane of transverse momentum vs normalized rapidity of protons in Ru+Ru collisions with the reaction cross section $\sigma_r \leqslant 72$ mb. Each successive contour line represents a relative factor of 2 in terms of yields. The thick solid lines show geometrical limits of the CDC and the HELITRON, the two drift chambers of the FOPI detector used in the present analysis ($32° \leqslant \theta_L \leqslant 140°$ and $9° \leqslant \theta_L \leqslant 26°$, respectively).

HELITRON covers $\theta_L = 9° - 26°$. An azimuthally symmetric Plastic Scintillator Wall covers $\theta_L = 1.2° - 30°$. In the CDC pions, protons, deuterons, and heavier particles are identified via the mean energy loss and the magnetic rigidity. In the overlapping angular range of the HELITRON and the Plastic Wall, particle identification is achieved by combining the magnetic rigidity determined with the HELITRON with the specific energy loss and time of flight from the Plastic Wall scintillators.

The details of the detector resolution and performance can be found in Refs. [12,23–25]. Figure 1 shows the phase space covered by the CDC and HELITRON for the identified protons in transverse momentum p_t (divided by the mass of proton m_p) and the normalized rapidity $y^{(0)}$:

$$y^{(0)} = y/y_{\text{c.m.}} - 1, \tag{1}$$

with $y_{\text{c.m.}}$ being the c.m. rapidity. Figure 1 shows that the FOPI detector covers a large portion of the full phase space at the beam energy investigated here. We use natural units $\hbar = c = 1$ in the following.

The centrality of each event is determined by the ratio E_{rat} of the total transverse ($E_\perp$) to longitudinal ($E_\parallel$) c.m. kinetic energies,

$$E_{rat} = \sum_i E_{\perp,i} \Big/ \sum_i E_{\parallel,i}, \tag{2}$$

where i runs over all charged particles detected in the CDC and the Plastic Wall. Previously, it has been demonstrated that E_{rat} is a suitable variable for event centrality, especially in central collisions at the present beam energy [10,26–28]. We note here that we have removed autocorrelation effects by excluding the ''particle of interest'' from the calculation

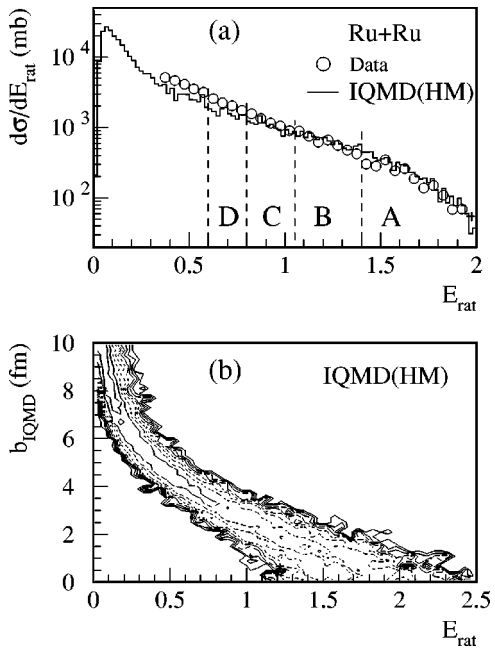

FIG. 2. (a) Experimental E_{rat} distribution (see text for details) in Ru+Ru collisions in comparison with IQMD(HM) model calculations. The labels A–D represent the centrality conditions which are utilized throughout this paper (cf. Table I). (b) Correlation between the impact parameter b_{IQMD} and E_{rat} in the IQMD(HM) model.

of E_{rat} when constructing E_{rat}-selected single particle observables such as rapidity distributions (Sec. III A). Autocorrelation effects on the momentum space topologies are sizeable only in the tails of the global observable (here, E_{rat}) [28] and cause a narrowing of the actual widths of rapidity distributions.

The upper panel of Fig. 2 shows the experimental E_{rat} distribution in Ru+Ru collisions compared with the result from the IQMD(HM) calculation, where H stands for the hard EoS option with a compressibility coefficient $K=380$ MeV and M for momentum dependent interaction (MDI). The model calculation was filtered by the geometrical acceptance of the detectors. In general, the model calculation agrees reasonably well with the data, especially in central collisions. The labels A–D represent the centrality conditions which will be used later in this paper. Table I summarizes the centrality criteria together with the experimental reaction cross section (σ_r), the geometrical impact parameter ($b_{geom}=\sqrt{\sigma_r/\pi}$) based on the sharp cutoff approximation, and the corresponding impact parameter range estimated by IQMD(HM) (b_{IQMD}). The bottom panel of Fig. 2 displays the correlation between the impact parameter b_{IQMD} and E_{rat} obtained by the IQMD(HM) model. It can be seen clearly that E_{rat} is a suitable variable for determining the centrality, especially for the most central collisions as the impact parameter approaches zero.

III. RESULTS

A. Proton and deuteron rapidity distributions

Figure 3 shows the invariant spectra, i.e., $(1/2\pi p_t)\cdot d^2N/dp_t dy^{(0)}$ vs p_t, of protons and deuterons at several rapidity windows selected by the $E_{rat}A$ condition in Ru+Ru collisions. In this figure two data sets obtained by two different detectors (CDC and HELITRON) are compared. For the HELITRON spectra, the matching efficiency between the HELITRON and the Plastic Wall, which was evaluated by comparing the number of tracks in the HELITRON with the number of hits in the Plastic Wall, was corrected. This efficiency is a function of θ_L: for $Z=1$ particles, it increases from ~40% at 9° to ~85% at 26°. The

TABLE I. Centrality bins of the E_{rat} distribution (denoted by $E_{rat}A$–$E_{rat}D$) with the corresponding reaction cross section σ_r for the present analysis of Ru+Ru collisions. The geometric impact parameter b_{geom} is determined by the sharp cutoff approximation. The impact parameters b_{IQMD} determined from the IQMD(HM) model are shown in the last column. The numbers represent the mean and one σ from a Gaussian fit except in case of the $E_{rat}A$ condition where the rms value is quoted, as it is impossible to fit a Gaussian function.

Centrality	E_{rat}	σ_r (mb)	b_{geom} (fm)	b_{IQMD} (fm)
$E_{rat}A$	$\geqslant 1.40$	$\leqslant 116$	$\leqslant 1.9$	0.9 ± 0.6
$E_{rat}B$	$1.05-1.40$	$116-235$	$1.9-2.7$	2.0 ± 0.5
$E_{rat}C$	$0.80-1.05$	$235-302$	$2.7-3.1$	2.9 ± 0.4
$E_{rat}D$	$0.60-0.80$	$302-432$	$3.1-3.7$	3.7 ± 0.4

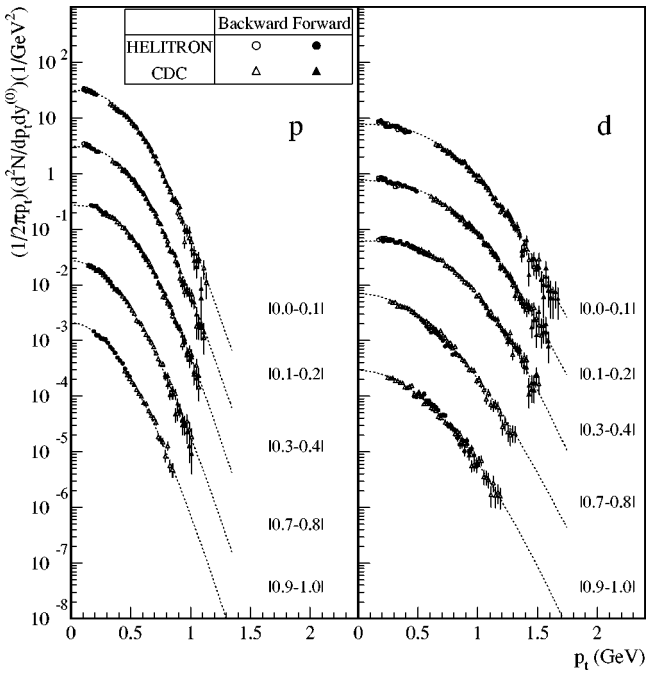

FIG. 3. Invariant spectra of protons and deuterons in Ru+Ru collisions for various rapidity bins ($E_{rat}A$ condition). Shown by dotted lines are the fits by a simple thermal blast model (see the text for the detailed functional form). Starting with the uppermost rapidity bin $|0.1-0.2|$, each successive spectrum has been multiplied by a decreasing power of 10 for a clearer display. The triangles and circles denote data from the CDC and HELITRON, respectively. Open and closed symbols represent the spectra in backward and forward hemispheres in c.m., respectively.

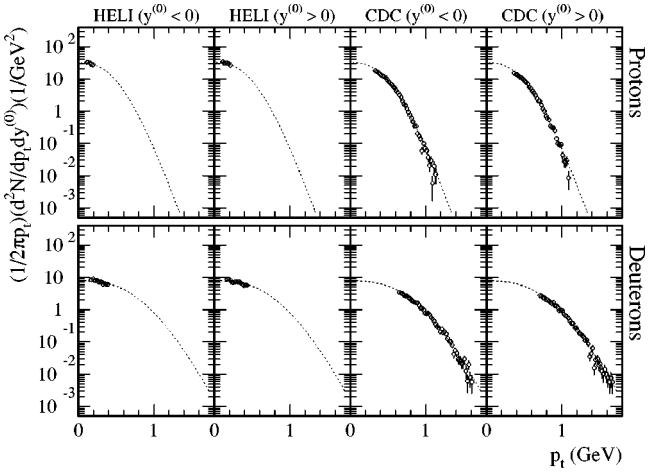

FIG. 4. Decomposed invariant spectra of protons (upper) and deuterons (lower part) in Ru+Ru collisions at midrapidity ($E_{rat}A$ condition). From the left to the right, the spectra represent the HELITRON backward, HELITRON forward, CDC backward, and CDC forward regions in c.m., respectively. Dotted lines are the fit functions of the simple thermal blast model.

CDC tracking efficiency of about 90% was also corrected for the spectra in Fig. 3. It was evaluated by using a full GEANT Monte Carlo simulation [29].

In Fig. 3, we observe a rather good matching between the spectra by the CDC and HELITRON within ~10% for protons and ~20% for deuterons at most. In addition, the spectra in the forward c.m. hemisphere are compared with those in the backward c.m. hemisphere in the phase-space region of overlap. In principle, they should be the same in symmetric collision systems such as Ru+Ru. Figure 3 demonstrates that this backward/forward symmetry can be verified well in this analysis. Since a distinction among spectra is not easy, we decompose, for example, the midrapidity invariant spectra of protons (upper panels) and deuterons (lower panels) in Fig. 4 for Ru+Ru collisions ($E_{rat}A$). In Fig. 4, from left to right, each individual spectrum represents the HELITRON backward, HELITRON forward, CDC backward, and CDC forward regions in c.m., respectively.

Also shown by dotted lines in Figs. 3 and 4 are the fits to the experimental invariant spectra by the simple thermal blast formula first proposed by Siemens and Rasmussen [30]:

$$\frac{1}{2\pi p_t}\frac{d^2N}{dp_t dy^{(0)}} \propto E e^{-\gamma_r E/T}\cdot\left[\left(\gamma_r + \frac{T}{E}\right)\frac{\sinh\alpha}{\alpha} - \frac{T}{E}\cosh\alpha\right], \tag{3}$$

where E and p are the total energy and momentum of the particle in the c.m. frame. Here $\gamma_r = 1/\sqrt{1-\beta_r^2}$ and $\alpha = (\gamma_r \cdot \beta_r \cdot p)/T$, while the radial flow velocity β_r and the thermal freeze-out temperature T are two free fit parameters. We fit spectra in the backward and forward hemispheres simultaneously using the reflection symmetry of the systems. The quality of the fit is good at all rapidities: the χ^2 per degree of freedom ranges from 0.8 to 1.5 for all rapidity bins independent of the collision centrality. The fit parameters at midrapidity ($|y^{(0)}| \leq 0.1$) [31] are shown in the first and second columns of Tables II for protons and III for deuterons at several centrality conditions. The fitting errors are negligibly small: less than 1% for both parameters for both particles. Note that the fit values of T are independent of the collision centrality, but β_r systematically decreases for peripheral collisions. In order to construct the $dN/dy^{(0)}$ spectra, we integrate the fit functions in Fig. 3 from 0 to ∞ in p_t to make up the missing p_t region (see Fig. 1). The fits with $\beta_r = 0$ are of poorer quality but the p_t-integrated yields are not much affected; this will be considered in the estimate of the systematic error (see below). Figure 5 shows the rapidity distributions of protons and deuterons in Ru+Ru collisions for four centrality conditions on E_{rat}. Note that our present rapidity distributions differ from those of the earlier publication by about 25% [22] (we mention in addition a scaling error of a factor 10 in Fig. 3 of Ref. [22]). Since the present analysis is based on an improved understanding of detector responses and takes into account HELITRON data as well as CDC data, the new data sets are taken to supersede the older data.

TABLE II. Fit parameters (T and β_r) for proton p_t spectra at midrapidity ($|y^{(0)}| \leq 0.1$) and total yield of protons per event under the different centrality conditions (cf. Table I). The fit errors for T and β_r are negligible, but the systematic error of the total yields is estimated to be about 9% (see text for details).

Centrality	$T(\|y^{(0)}\| \leq 0.1)$ (MeV)	$\beta_r(\|y^{(0)}\| \leq 0.1)$	Total yield
$E_{rat}A$	38.4	0.32	31.2
$E_{rat}B$	39.8	0.32	29.6
$E_{rat}C$	39.7	0.30	27.2
$E_{rat}D$	39.2	0.29	24.6

The estimate of the systematic error affecting the overall normalization of the p_t-integrated yields of the $dN/dy^{(0)}$ values of protons and deuterons includes the following considerations: (i) track quality cut (3%), (ii) strategy for the HELITRON momentum reconstruction (with and without including the event vertex) (2%), (iii) fit functions by comparing the results obtained by Eq. (3) and a purely thermal ($\beta_r = 0$) Boltzmann function (3%), (iv) discrepancy between the CDC and HELITRON spectra (Fig. 3) in the overlapped phase-space region (5%), and (v) uncertainty in track reconstruction efficiency (5% for protons and 9% for deuterons). As a result, we estimate the systematic error of the overall normalization of the $dN/dy^{(0)}$ distributions to be at most

TABLE III. Fit parameters (T and β_r) for deuteron p_t spectra at midrapidity ($|y^{(0)}| \leq 0.1$) and total yield of deuterons per event under the different centrality conditions. The fit errors for T and β_r are negligible, but the systematic error of the total yields is estimated to be about 11% (see text for details).

Centrality	$T(\|y^{(0)}\| \leq 0.1)$ (MeV)	$\beta_r(\|y^{(0)}\| \leq 0.1)$	Total yield
$E_{rat}A$	49.1	0.26	17.2
$E_{rat}B$	50.1	0.25	16.0
$E_{rat}C$	48.7	0.24	14.8
$E_{rat}D$	49.4	0.22	13.0

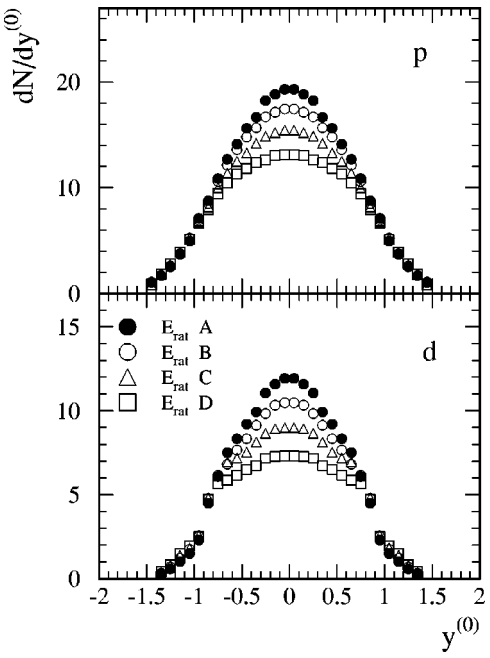

FIG. 5. Centrality dependence of the proton and deuteron rapidity distributions for the various centrality cuts in Ru+Ru collisions.

about 9% and 11% for protons and deuterons, respectively, which is the quadratic sum of all the listed errors.

Since our fitting function, Eq. (3), does not account for possible low-p_t spectator components near rapidities $y^{(0)} = \pm 1$, we expect the tails of the rapidity distributions for noncentral collisions to be representative only for participant matter. As can be seen in the acceptance plot of Fig. 1, low-p_t parts of the spectra near target/projectile rapidity, most likely to be populated by spectator fragments, are not covered in the isotope separated distributions. With use of the information from the Plastic Wall which allows charge, but not isotope, separation of fragments down to 1.2°, we were able to check that our fitting procedure was fully adequate for central collisions (of main interest), and that the data in the range $|y^{(0)}| \leq 0.7$ were unaffected also for the more peripheral collisions. To further confirm that our estimation by the extrapolation procedure over the full phase space is reasonable, we have checked that the total charge of all reaction products agrees with the initial charge in the system (88 in Ru+Ru collisions) within 5% [32] for central collisions.

In Fig. 5, we observe that protons and deutrons are concentrated more at midrapidity for more central collisions. The last columns of Tables II and III summarize the rapidity—and p_t-integrated yields of protons and deuterons, respectively, for four different centralities. The ratio of deuteron and proton yields is about 54% in Ru+Ru collisions independent of centrality. This should be compared with about 72% estimated in Au+Au collisions at the same beam energy [28].

The comparison of the experimental $dN/dy^{(0)}$ spectrum for the most central event criterion ($E_{rat}A$) with the IQMD(HM) calculations ($b_{IQMD} \leq 1$ fm) is shown in Fig. 6. Four assumptions on σ_{NN} in the model are used. In the IQMD transport approach, composite particles are produced

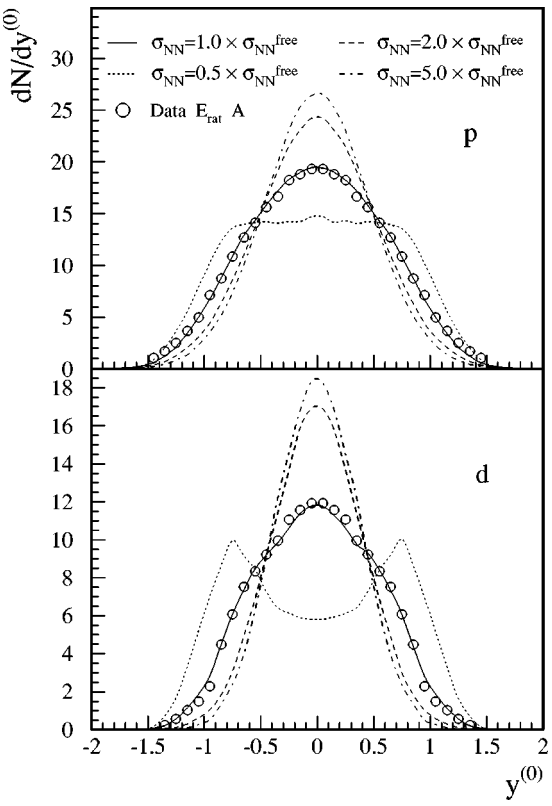

FIG. 6. Comparison of the proton and deuteron rapidity distributions in Ru+Ru collisions (open circles) with the results from the IQMD(HM) calculations (various lines). Data are for the $E_{rat}A$ criterion, and the model calculations are for $b_{IQMD} \leq 1$ fm and values of σ_{NN} between $0.5\sigma_{NN}^{free}$ and $5\sigma_{NN}^{free}$.

by a coordinate space cluster algorithm. With default parameters, the algorithm starts to produce composite particles, including deuterons, after 200 fm in time, and it is well known that too few composites are produced in the standard IQMD [28]. Therefore, we emphasize only the spectral shapes of protons and deuterons, but not the absolute yields in the model. All model calculations are normalized in such a way that the integration of $dN/dy^{(0)}$ is the same as in the data. In Fig. 6 we find that the experimental proton and deuteron $dN/dy^{(0)}$ distributions are in best agreement with the $\sigma_{NN} = \sigma_{NN}^{free}$ assumption. Choices of other σ_{NN} options, deviating by more than 20% from the free value, can be excluded from later considerations (in this context, one should realize that IQMD, as most other transport calculations, takes Pauli blocking into account in an approximate way [10]).

In particular, in the mid-1970's, it was argued that hydrodynamics in nucleus-nucleus collisions was governed by the shock waves propagating in the beam direction [33]. Shock waves can be generated when the border of the stopped matter moves faster than the speed of sound in nuclear matter. In an ideal hydrodynamics, it was predicted that shock waves would be generated in the early time of collisions and the nuclear matter is pushed outwards perpendicular to the beam direction (transverse expansion) [33]. However, such a transverse expansion turns out to be absent in the polar angle distributions of data at beam energy $\leq 400A$ MeV [28]. In

TABLE IV. Mean rapidity shift of protons normalized to beam rapidity ($\delta y_p/y_b$). Upper part: Experimental values for the four centrality bins, lower part: IQMD model results for $b \leqslant 1$ fm and different parameters of $\sigma_{NN}/\sigma_{NN}^{free}$.

	Centrality	$\sigma_{NN}/\sigma_{NN}^{free}$	$\delta y_p/y_b$
	$E_{rat}A$		0.256 ± 0.011
Data	$E_{rat}B$		0.250 ± 0.011
	$E_{rat}C$		0.244 ± 0.010
	$E_{rat}D$		0.234 ± 0.010
		5.0	0.312 ± 0.013
IQMD(HM)	$b_{IQMD} \leqslant 1$ fm	2.0	0.295 ± 0.012
		1.0	0.261 ± 0.010
		0.5	0.215 ± 0.009

microscopic transport approaches, e.g., IQMD [10,26], one can imitate ideal hydrodynamics by strongly increasing σ_{NN} in the medium. Alternatively, one can simulate transparency by using very small values of σ_{NN}. In Fig. 6 we also show the proton and deuteron $dN/dy^{(0)}$ spectra from IQMD in two extreme cases for small and large σ_{NN} values, respectively. The spectrum which is most elongated longitudinally is for $0.5\sigma_{NN}^{free}$, whereas the spectrum which is highly concentrated at midrapidity, due to the transverse expansion, is obtained for $5\sigma_{NN}^{free}$. In the latter case, nuclear matter rebounds after instant equilibration mimicking the effects by the shock wave in hydrodynamics (see also Sec. III C and Fig. 8 below). It is obvious that the two extreme scenarios (high transparency and the validity of an ideal hydrodynamics scenario) can be completely excluded by our data.

B. Mean rapidity shifts and the search for scaling properties

In order to quantify the widths of $dN/dy^{(0)}$ distributions, we utilize the mean rapidity shift of protons, δy_p, defined by [12]

$$\delta y_p \equiv \frac{\int_{-\infty(0)}^{0(\infty)} |y^{(0)} - y_{t(b)}| (dN/dy^{(0)}) dy^{(0)}}{\int_{-\infty(0)}^{0(\infty)} (dN/dy^{(0)}) dy^{(0)}}, \qquad (4)$$

TABLE V. Same as Table IV, but for deuterons.

	Centrality	$\sigma_{NN}/\sigma_{NN}^{free}$	$\delta y_p/y_b$
	$E_{rat}A$		0.287 ± 0.012
Data	$E_{rat}B$		0.277 ± 0.011
	$E_{rat}C$		0.266 ± 0.011
	$E_{rat}D$		0.254 ± 0.010
		5.0	0.352 ± 0.014
IQMD(HM)	$b_{IQMD} \leqslant 1$ fm	2.0	0.338 ± 0.014
		1.0	0.282 ± 0.011
		0.5	0.192 ± 0.008

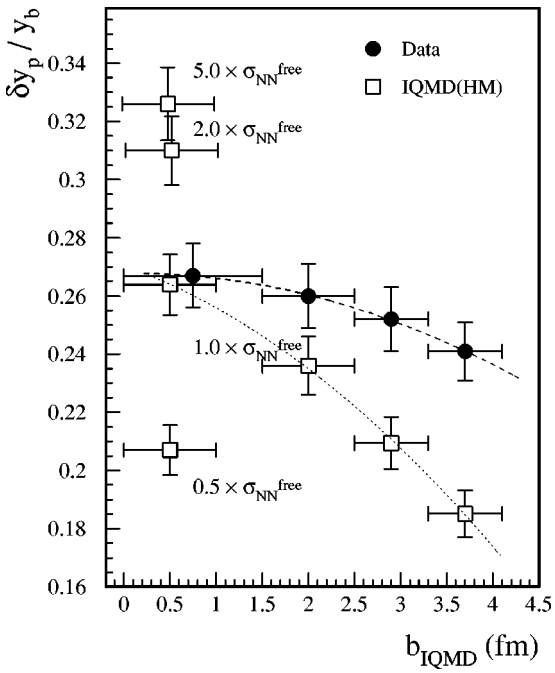

FIG. 7. Comparison of experimental (closed) and calculated [IQMD(HM) model, open symbols] mean rapidity shifts of protons normalized to beam rapidity ($\delta y_p/y_b$) as a function of the impact parameter. As indicated various assumptions on σ_{NN} have been used in the calculations. The dashed and dotted lines are second order polynomial fits to the data and calculations, respectively.

where y_t and y_b represent target and beam rapidities, respectively. Note that the variable δy_p becomes larger for narrower rapidity distributions. Quantitatively, the variable δy_p normalized to y_b decreases by about 2% and 4% for protons and deuterons, respectively, by removing the autocorrelation effect. We use this variable in order to facilitate a detailed comparison between the measured $dN/dy^{(0)}$ shapes and those of the model calculations.

The experimental δy_p values within the four analyzed centrality bins are summarized in the upper parts of Table IV for protons and in Table V for deuterons; they are normalized to y_b. As expected in a transparency scenario, $\delta y_p/y_b$ is larger for more central collisions (it should be smaller in a longitudinally expanding fireball scenario). Furthermore, the $\delta y_p/y_b$ value for deuterons is larger than for protons in a given centrality bin, which agrees with the IQMD calculations. The lower parts of both tables give the $\delta y_p/y_b$ results of the IQMD model for both particles in the centrality bin $b_{IQMD} \leqslant 1$ fm, calculated for four different values of $\sigma_{NN}/\sigma_{NN}^{free}$.

Figure 7 summarizes these results; each point is the weighted mean of the corresponding proton and deuteron $\delta y_p/y_b$ values. As in the tables the measured values for the four centrality bins are shown together with the IQMD results calculated for the most central bin with the different choices of $\sigma_{NN}/\sigma_{NN}^{free}$. For the case $\sigma_{NN}/\sigma_{NN}^{free} = 1$ the calculated centrality dependence is shown in addition. For the most central collisions the measured value is reproduced by the assumption of the total nucleon-nucleon cross section in a dense and hot environment agreeing with the free value

σ_{NN}^{free}. This is consistent with conclusions from the isospin tracer method that excluded a significant reduction of σ_{NN} in the medium [22] (see also Sec. III C). A discrepancy is observed, however, in the centrality dependence of $\delta y_p/y_b$: as the impact parameter increases the IQMD calculations show a much faster drop of $\delta y_p/y_b$ than do the data.

At this point, the use of the stiff EoS with MDI in the IQMD calculations shown so far is deserving of more attention. Very similar proton rapidity distributions can be obtained in IQMD without MDI if the stiff EoS is replaced by a soft one (compressibility coefficient $K=200$ MeV). With $\sigma_{NN}=\sigma_{NN}^{free}$, the variable $\delta y_p/y_b$ for the soft EoS with MDI is 0.263 ± 0.011, within the errors identical to the result with the hard EoS (0.261 ± 0.010, cf. Table IV) [34]. For the same σ_{NN} we obtain $\delta y_p/y_b=0.276\pm0.011$ if we switch off MDI but keep the hard EoS; this is somewhat larger ($\sim$6%) than the observed value in the data [narrower $dN/dy^{(0)}$ distribution]. Although the different choice of MDI seems to influence the proton $dN/dy^{(0)}$ distribution more than the choice of the EoS, we conclude that, irrespective of the various options on the EoS and MDI, the agreement between the model and the Ru+Ru data at 400*A* MeV is best (within their systematic errors) when σ_{NN} is chosen very close to σ_{NN}^{free}.

Finally, the effect of the Gaussian packet width of the particles (L) in the IQMD calculation also deserves some attention [35]. In the model it is expected that different values of L lead to different interaction lengths. For this theoretical parameter we have used a standard value of 8.66 fm^2 which was optimized for relatively heavy collision systems such as Au+Au. For light collision systems half of this value (4.33 fm^2) was suggested, as this parameter was important for the study of the transition energy [36]. Therefore, we have checked the effect of the Gaussian packet width of particles on the shape of the baryon rapidity distributions. We observe that the widths of the proton and deuteron rapidity spectra are almost the same (within 1% in the $\delta y_p/y_b$ representation) for both values of L for $\sigma_{NN}\geqslant\sigma_{NN}^{free}$ options in central collisions. As an example, we obtain $\delta y_p/y_b=0.268$ and 0.266 for $L=8.66$ and 4.33 fm^2, respectively, for $\sigma_{NN}=\sigma_{NN}^{free}$. This difference becomes even smaller for larger values of σ_{NN}. A noticeable effect is found only for $\sigma_{NN}=0.5\sigma_{NN}^{free}$, where $\delta y_p/y_b$ is about 8% larger for a smaller packet width. As a result, we conclude that the width of the Gaussian packet cannot change our conclusion on nuclear stopping phenomena, even though its contribution is important for studying the transition energy.

The systematics of the baryon rapidity losses has been discussed by Videbæk and Hansen for central nucleus-nucleus collisions in a beam energy range from 10*A* to 200*A* GeV [37] and has been extended down to 1*A* GeV in Ref. [12]. The important conclusion was that the mean rapidity shift δy_p of protons scaled with the beam rapidity y_b from 1*A* to 200*A* GeV. With the present results this scaling behavior can be tested further at 400*A* MeV. Our weighted mean of $\delta y_p/y_b$ for both protons and deuterons in Ru+Ru collisions is 0.267 ± 0.011 within the $E_{rat}A$ cut. It agrees reasonably with the average $\delta y_p/y_b$ value (0.28) of relatively small collision systems ($A\leqslant58$) from 1*A* to 200*A* GeV and is about 15% smaller than that of Au+Au collisions at 11*A* GeV [12]. Assuming the scaling law holds from 400*A* MeV to 200*A* GeV, we can see the system size dependence: the larger collision system shows a larger value of $\delta y_p/y_b$, which implies more concentration of protons at midrapidity. However, a definite conclusion can be drawn only after the proton $dN/dy^{(0)}$ distributions for $A\sim100$ are available at other beam energies.

C. Ratio of rapidity distributions in isospin asymmetric systems

Incomplete stopping in heavy-ion collisions, evidenced by the present data in comparison with transport calculations, suggests that complete thermal equilibration may not be achieved. Such conclusions were reached more unambiguously (i.e., in principle, without the need for the transport model calculations) by our collaboration by using the *isospin tracer method* [22] which is based on a combined study of four systems: two symmetric ones, Ru+Ru and Zr+Zr, and two mixed systems, Ru+Zr and Zr+Ru (inverting projectile and target). The following observable was studied in Ref. [22]:

$$R_Z=\frac{2N_y^{mix}-N_y^{\mathrm{Zr}}-N_y^{\mathrm{Ru}}}{N_y^{\mathrm{Zr}}-N_y^{\mathrm{Ru}}}, \tag{5}$$

where N_y^i is the differential yield in the detector acceptance at a given rapidity y for mass symmetric systems (Zr+Zr with $i=$Zr, Ru+Ru with $i=$Ru, and the mixed systems Ru+Zr, respectively, Zr+Ru with $i=$mix). This observable was designed to assess the differential rapidity distribution for protonlike ejectiles relative to that of the corresponding ''calibrating'' symmetric systems.

To illuminate further our earlier results we present here data for a related, but simpler, observable, which involves only the mixed systems

$$R_p=\frac{N_y^{\mathrm{Ru+Zr}}}{N_y^{\mathrm{Zr+Ru}}}, \tag{6}$$

i.e., simply the ratio of the differential rapidity distributions for the two mixed systems (distinguished by exchanging projectile and target). This simple ratio gives us a clean signal about the nuclear stopping phenomenon via the sign of the slope near midrapidity. The ratio R_p will show different behavior as a function of rapidity for different nuclear stopping scenarios: R_p increases as a function of rapidity (positive slope) for transparency and decreases (negative slope) for rebound. If full mixing of isospin has been achieved in the collision, R_p (as well as R_Z) as a function of rapidity is expected to be flat.

Open circles in Fig. 8 show R_p values measured in the CDC for protons under the $E_{rat}A$ condition. The fact that R_p crosses unity at midrapidity is an important consistency check, since an equal number of projectile and target nucleons should be admixed in c.m. due to the mass symmetry of the collision systems. The ratios R_Z and R_p are less prone to

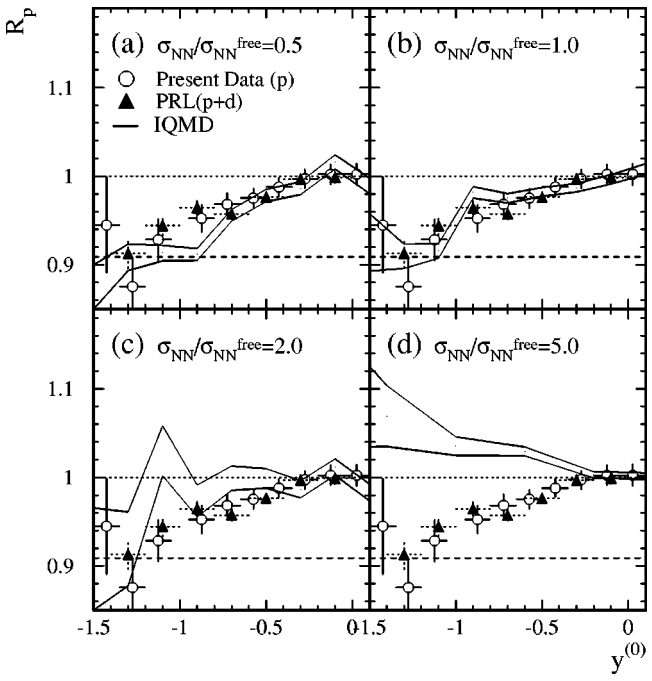

FIG. 8. Comparison of the experimental R_p (see text for details) obtained from the CDC under $E_{rat}A$ criterion with the results from the IQMD(HM) calculations. Open circles are the present experimental data, and thin solid lines are the limits estimated by the model calculations. The nucleon-nucleon cross section σ_{NN} in the model was assumed to be (a) 0.5, (b) 1, (c) 2, and (d) 5 times σ_{NN}^{free}. Solid triangles reflect earlier results obtained from the protonlike particle $(p+d)$ ratio in the CDC alone (Ref. [22]). The dashed line represents the lower limit of R_p determined by the N/Z ratio of projectile and target nuclei, if R_p were to include all protons, bound or not.

systematic errors than the rapidity distributions themselves because the ratio eliminates many systematic uncertainties due to an imperfect detector response. Specifically, by exchanging target and projectile in an (isospin) asymmetric system it is technically possible to measure the backward and the forward hemispheres (in the center of mass) with the same subdetectors.

Results deduced from the earlier rapidity distribution evaluation [22] that included the sum of the protons and the deuterons, are also shown for comparison in Fig. 8 (solid triangles). The current results agree nicely with the previous results confirming the robustness of this observable to changes in the analysis. In contrast, the absolute rapidity distributions, $dN/dy^{(0)}$, of protons and deuterons are now found to differ from the earlier analysis by typically 25%. However, this change in $dN/dy^{(0)}$ does not affect the main conclusions of Ref. [22] which were based primarily on the robust observable R_Z.

Furthermore, such a good agreement between the previous result for the sum of protons and deuterons and the present result only for protons (Fig. 8) also means that the ratios R_p of both particles are very similar. We have checked that adding deuterons in R_p does not change the shape of the experimental data shown in Fig. 8. In addition, the possible bias due to the pion production was investigated by the pion ratios for both charges. Within statistical errors, the ratio R_π is consistent with unity for both π^+ and π^-, and no signature of finite slope is found at this beam energy. A detailed study of R_π for various nuclear stopping scenarios will be published in a separate paper.

The behavior of the experimental quantity R_p in Fig. 8 is qualitatively in agreement with the ''transparency'' scenario for central collisions as R_p increases with $y^{(0)}$. Experimentally, we cannot separate the corona effect (surface nucleons of the colliding nuclei passing through each other) from the bulk transparency of the system. However, we expect that such corona effects become important only close to the projectile and target rapidities, which has been also confirmed by the CBUU model [19]. Therefore, the finite slope of R_p near *midrapidity* suggests a partial bulk transparency of the projectile and target nuclei.

The ratios R_p from the IQMD(HM) model are shown by thin solid lines in Fig. 8 for various assumptions on σ_{NN}, always under the most central cut $b_{IQMD} \leqslant 1$ fm. They are corrected for the geometrical acceptance of the detector. This is a small correction, however; the effect is that the acceptance is almost negligible since the analysis relies on a relative quantity. From our present investigations, the degree of nuclear stopping is found to be rather sensitive to σ_{NN} in IQMD. In order to study the details of the effect of this parameter, we compare again experimental R_p data with model calculations for various σ_{NN}. The agreement is reasonably good for both $\sigma_{NN}=0.5\sigma_{NN}^{free}$ and σ_{NN}^{free} options, especially for $|y^{(0)}| \leqslant 0.5$ which is the most interesting region for the nuclear stopping phenomenon. The option $\sigma_{NN}=0.5\sigma_{NN}^{free}$ has already been excluded in the previous section by the comparison to the experimental proton and deuteron rapidity distributions. The model predicts that the isospin equilibrium can be achieved if σ_{NN} becomes close to $2\sigma_{NN}^{free}$. Finally, the model calculation with $\sigma_{NN}=5\sigma_{NN}^{free}$ shows a *negative* slope which implies a rebound effect predicted by an ideal hydrodynamic model [33], an effect which is clearly excluded by the R_p and R_Z data, as well as by the rapidity distributions discussed earlier.

IV. CONCLUSIONS

We have used two experimental observables to study the nuclear stopping phenomenon at 400*A* MeV. The first, conventional, observable is the proton and deuteron rapidity distributions, analyzed in Ru+Ru collisions, and the second one is the ratio of proton rapidity distributions in isospin asymmetric collisions of the isobaric nuclei Ru+Zr and Zr+Ru.

These two observables are truly complementary. The baryon rapidity spectra enable us to estimate the mean rapidity shift of protons. By comparison to model calculations one can further confine quantitatively the magnitude of *NN* cross section in the nuclear medium. However, one shortcoming of this method is that we cannot distinguish in a model-independent way between various stopping scenarios such as transparency, rebound, and longitudinal expansion after a complete mixing of projectile and target nucleons. On the other hand, the ratio of proton rapidity distributions in isospin asymmetric systems gives us a tool to resolve such an

ambiguity despite its relatively small sensitivity to determine the *NN* cross section precisely.

From the centrality dependence of proton and deuteron rapidity distributions, we find that more protons are concentrated at midrapidity for more central events (the shape of the rapidity distribution is narrower). Expressed in terms of nuclear stopping, more stopping can be achieved in more central events. To reproduce the proton and deuteron rapidity distributions for the most central events measured experimentally, the *NN* cross section in dense and hot nuclear matter should remain within about 20% of the free *NN* cross section within the framework of IQMD. With this constraint, the ratio of proton rapidity distributions in Ru+Zr and Zr+Ru collisions evidences a partial transparency effect of nuclei at 400*A* MeV.

Since nuclear stopping depends on the system size and beam energy, we cannot generalize the present conclusion to other collision systems and incident energies. However, the method we utilized in this experiment should be applicable and robust to all nucleus-nucleus collisions in general. Data at 1.5*A* GeV for the same collision systems are being presently analyzed, and the beam energy dependence of the nuclear stopping phenomenon is the subject of a forthcoming paper.

ACKNOWLEDGMENTS

We gratefully acknowledge support from the Korea Science and Engineering Foundation (KOSEF) under Project No. 20015-111-01-2, Deutsche Forschungsgemeinschaft (DFG) under Project No. 446 KOR-113/76/0, and the French-German agreement between GSI and IN2P3/CEA.

[1] R. Stock, Phys. Rep. **135**, 259 (1986).
[2] H. Stöcker and W. Greiner, Phys. Rep. **137**, 277 (1986).
[3] P. Senger and H. Ströbele, J. Phys. G **25**, R59 (1999).
[4] W. Reisdorf and H.G. Ritter, Annu. Rev. Nucl. Part. Sci. **47**, 663 (1997).
[5] J.-Y. Ollitrault, Nucl. Phys. **A638**, 195c (1998).
[6] G.E. Brown, Phys. Rep. **163**, 167 (1988).
[7] C.M. Ko and G.Q. Li, J. Phys. G **22**, 1673 (1996).
[8] J. Cleymans and K. Redlich, Phys. Rev. C **60**, 054908 (1999).
[9] P. Braun-Munzinger, J. Stachel, J.P. Wessels, and N. Xu, Phys. Lett. B **344**, 43 (1995).
[10] J. Aichelin, Phys. Rep. **202**, 233 (1991).
[11] G.F. Bertsch and S. Das Gupta, Phys. Rep. **160**, 189 (1998).
[12] FOPI Collaboration, B. Hong *et al.*, Phys. Rev. C **57**, 244 (1998); **58**, 603 (1998).
[13] E814 Collaboration, J. Barrette *et al.*, Phys. Rev. C **50**, 3047 (1994).
[14] E877 Collaboration, J. Barrette *et al.*, Phys. Rev. C **62**, 024901 (2000).
[15] NA44 Collaboration, I.G. Bearden *et al.*, Phys. Lett. B **388**, 431 (1996).
[16] NA49 Collaboration, H. Appelshauser *et al.*, Phys. Rev. Lett. **82**, 2471 (1999).
[17] S. A. Bass, J. Konopka, M. Bleicher, H. Stöcker, and W. Greiner, *GSI Scientific Report 94-1* (GSI, Germany, 1995), p. 66.
[18] B.A. Li, C.M. Ko, and W. Bauer, Int. J. Mod. Phys. E **7**, 147 (1998).
[19] A. Hombach, W. Cassing, and U. Mosel, Eur. Phys. J. A **5**, 77 (1999).
[20] S.J. Yennello *et al.*, Phys. Lett. B **321**, 15 (1994).
[21] B.A. Li and S.J. Yennello, Phys. Rev. C **52**, R1746 (1995).
[22] FOPI Collaboration, F. Rami *et al.*, Phys. Rev. Lett. **84**, 1120 (2000).
[23] FOPI Collaboration, A. Gobbi *et al.*, Nucl. Instrum. Methods Phys. Res. A **324**, 156 (1993).
[24] J. Ritman for the FOPI Collaboration, Nucl. Phys. B (Proc. Suppl.) **B44**, 708 (1995).
[25] FOPI Collaboration, D. Best *et al.*, Nucl. Phys. **A625**, 307 (1997).
[26] C. Hartnack, Rajeev K. Puri, J. Aichelin, J. Konopka, S.A. Bass, H. Stöcker, and W. Greiner, Eur. Phys. J. A **1**, 151 (1998).
[27] FOPI Collaboration, S.C. Jeong *et al.*, Phys. Rev. Lett. **72**, 3468 (1994).
[28] FOPI Collaboration, W. Reisdorf *et al.*, Nucl. Phys. **A612**, 493 (1997).
[29] GEANT-Detector Description and Simulation Tool, CERN Program Library Long Writeup W5013 (CN Division, CERN, 1993).
[30] P.J. Siemens and J.O. Rasmussen, Phys. Rev. Lett. **42**, 880 (1979).
[31] At 400*A* MeV the produced particles show very isotropic source shape in the c.m. frame in Au+Au collisions (Ref. [28]). Since we look at the p_t spectra in a constant rapidity bin in this analysis, the fit parameters may be meaningful only at midrapidity, assuming the source shape is also isotropic in Ru+Ru collisions.
[32] FOPI Collaboration, W. Reisdorf *et al.* (to be published).
[33] W. Scheid, H. Müller, and W. Greiner, Phys. Rev. Lett. **32**, 741 (1974).
[34] For larger collision systems such as Au+Au, the softer EoS makes the $dN/dy^{(0)}$ distribution of protons and fragments somewhat wider, e.g., see G. Peilert, H. Stöcker, W. Greiner, A. Rosenhauer, A. Bohnet, and J. Aichelin, Phys. Rev. C **39**, 1402 (1989).
[35] C. Hartnack, Ph.D. thesis, Frankfurt University, 1992.
[36] S. Soff, S.A. Bass, C. Hartnack, H. Stöcker, and W. Greiner, Phys. Rev. C **51**, 3320 (1995).
[37] F. Videbæk and O. Hansen, Phys. Rev. C **52**, 2684 (1995).